Accepted for publication in *Ceramics International*, 2015.

Microwave-Plasma Synthesis of Nano-sized Silicon Carbide at Atmospheric Pressure

JH van Laar[1*], JFM Slabber[1], JP Meyer[1], IJ vd Walt[2], GJ Puts[3], PL Crouse[3]

[1]*Thermoflow Group, Department of Mechanical Engineering, Faculty of Engineering, Built Environment and Information Technology, University of Pretoria, Pretoria, South Africa*

[2]*Applied Chemistry Division, South African Nuclear Energy Corporation (NECSA), Pelindaba, North West Province, South Africa*

[3]*Fluoro-Materials Group, Department of Chemical Engineering, Faculty of Engineering, Built Environment and Information Technology, University of Pretoria, Pretoria, South Africa*

**Corresponding Author: Tel.: +2771 898 6674, E-mail address: jean@vanlaar.co.za*

Abstract

A microwave plasma process operating at atmospheric pressure was developed for the synthesis of SiC nanoparticles. The process utilizes methyltrichlorosilane (MTS) as precursor, acting as both carbon and silicon source, along with an additional hydrogen feed to ensure a fully reducing reaction environment. In addition, argon served as carrier gas.. The parameters studied were the H_2:MTS molar ratio and the total enthalpy, in the range 0 to 10 and 70 to 220 MJ/kg respectively. The particles size distribution ranged from 15 to 140 nm as determined by SEM and TEM micrographs. It was found that an increase in enthalpy and a higher H_2:MTS ratio resulted in smaller SiC particle sizes. The adhesion of particles was a common ocuurence during the process, resulting in larger agglomerate sizes.

Keywords: silicon carbide, microwave plasma, nanoparticles, methyltrichlorosilane

1. Introduction

The favourable physical and mechanical properties of silicon carbide (SiC) allow for various applications across many areas, e.g. in high power and high frequency electronics as well as high temperature technologies [1,2]. At present the material is receiving increased attention as a nuclear ceramic due to its excellent mechanical properties, low neutron absorption cross-section (25% that of zirconium based alloys) and dimensional stability under irradiation [3]. While conventional carbide ceramics exhibit certain drawbacks, such as low ductility and high brittleness, nano-sized carbide powders can easily overcome these shortcomings.

SiC nanoparticles have been shown to exhibit properties that differ substantially from that of the bulk material, encouraging the creation of new areas of application. Many different maufacturing methods for the creation of SiC nanoparticles have been reported in the literature. These include carbothermic reduction [4], pulsed laser deposition [5], sol-gel processes [6], microwave heating [7,8] as well as different plasma techniques such as inductive radio-frequency (RF) [9]–[11], direct current (DC) thermal [12], low pressure microwave plasmas [13] and microwave plasma assisted chemical vapour deposition [14,15]. Vennekamp et al. [16] described the formation of a SiC nanopowder using an atmospheric microwave plasma with tetramethylsilane (TMS) as precursor. They also produced growth-rate equations using the concept of Ostwald ripening, showing the dependency of particle growth rate on temperature and pressure. Microwave plasmas have also been used for the synthesis of other nanoscale substances such as Si [17], MoS_2 and WS_2 [18], WO_3 [19] and Zn and ZnO [20].

It is well known that, given the right conditions, methyltrichlorosilane (CH_3SiCl_3 or MTS) decomposes to form SiC and hydrogen chloride (HCl) shown in Equation 1.

$$CH_3SiCl_3 \rightarrow SiC + 3HCl \quad (1)$$

The reaction kinetics and mechanisms of this reaction have been thoroughly reported in the literature through chemical vapour deposition [21]–[24], chemical vapour infiltration [25], radio frequency induction plasma [26] and pyrolysis [27] investigations. In this paper the synthesis of SiC nanoparticles from MTS is reported using a microwave-induced plasma, operating at atmospheric pressure in an argon/hydrogen environment. Operation at atmospheric pressure allows for the possible development of low cost, less energy intensive

synthesis methods and smaller equipment footprints. MTS was used as feed material due to the benefit of having a stoichiometric silicon-to-carbon elemental ratio, and the relative ease of the procedure through which MTS can be fed into the system due to its liquid state and high vapour pressure at standard conditions and high volatility.. Hydrogen was fed into the reactor along with the MTS as a reductant to drive the conversion reaction. The process parameters studied were the H_2:MTS molar ratio and the total enthalpy. Argon served as the carrier gas for MTS.

2. Experimental

2.1 Apparatus

A commercial microwave source from Electronic GmbH & Co., Germany, model PGEN2450/1.5-1.5KW2AIW, was used. The equipment consists of a 1500 W power supply with a MOS-FET amplifier, a microwave generator operating at 2.45 GHz, a water-cooled magnetron head, a stub tuner, a rectangular waveguide and a sliding short. The quartz tube, in which the plasma is generated and maintained, was positioned through the middle- and perpendicular to the wave guide before the stub tuner. The quartz tube has an internal diameter of 2 cm and a length of 30 cm. An in- and outlet at the top and bottom of the quartz tube allows for the flow of gas through the plasma. The tube was cooled by blowing air into an inlet into the waveguide perpendicular to the quartz tube and letting the air pass over the tube, exiting through the top and bottom openings in the waveguide. Argon and hydrogen flow rates were controlled using Aalborg rotameters. The physical layout of the reactor assembly is illustrated in Figure 1 and a schematic representation of the flow path is shown in Figure 2.

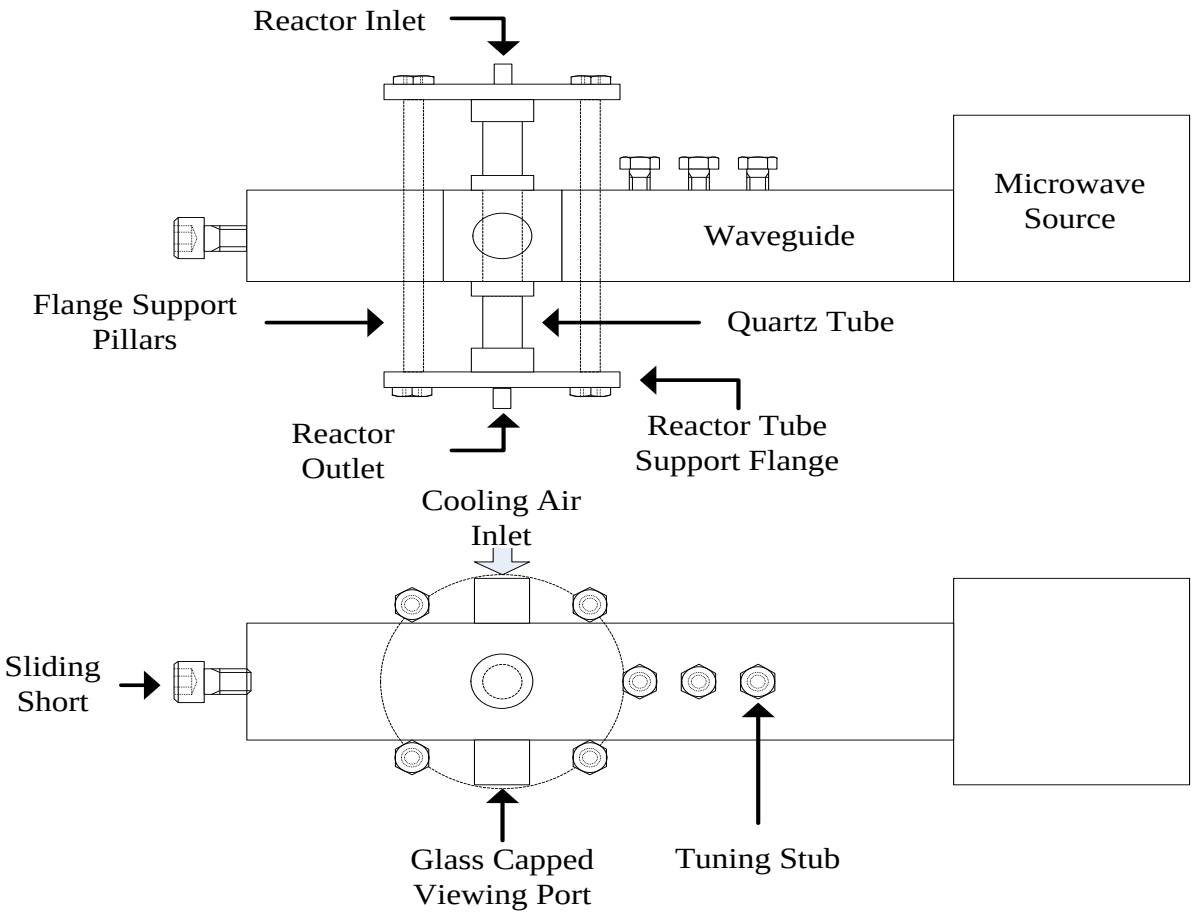

Figure 1: Physical layout of the reactor assembly.

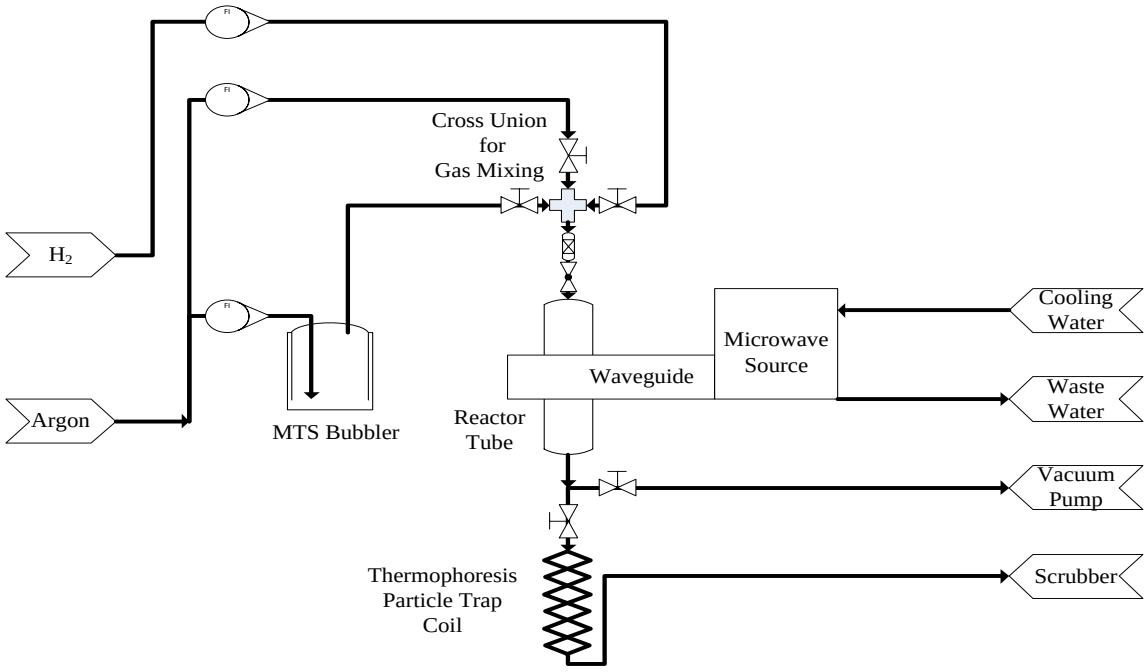

Figure 2: Schematic representation of the flow path of the experimental assembly.

MTS vapour was fed into the reactor by vaporising MTS into a bypass argon stream and passing the MTS laden argon into a cross joint where it was mixed with the main argon stream and the hydrogen feed. The total gaseous feed mixture was passed through a 0.2 micron sintered metal filter to ensure that no solid materials enter the plasma reactor and that the total gas mixture is homogenously mixed. The mass flow of MTS was controlled by varying the bubbling rate of the argon carrier.. The MTS mass transfer as a function of argon flow rate in standard cubic centimeters per minute (sccm) is shown in Figure 3. The calibration curve was determined by bubbling argon through the liquid MTS at different flow rates for 10 minutes each, and measuring the mass difference after each run.

The MTS vaporisation assembly consisted of a 250 mL borosilicate glass jar equipped with a lid containing an inlet and outlet port. The argon inlet line was placed below the level of the MTS. The inlet line was left open and the argon allowed to bubble freely.

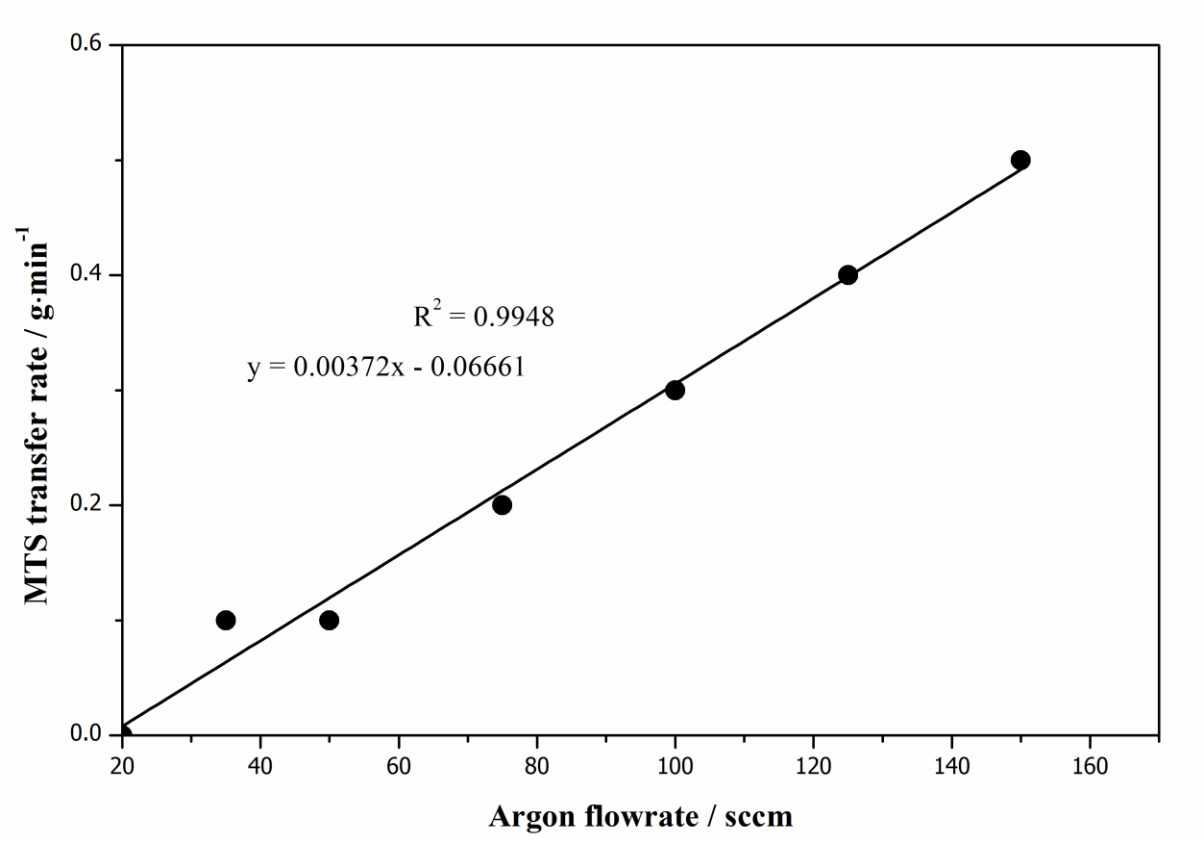

Figure 3: MTS mass transfer calibration curve.

Some physical properties of MTS are given in **Table 1** [28].

Table 1: Physical properties of MTS [28].

Property	Value	Units
Molecular weight	149.48	g/m
Boiling point	65	°C
Melting point	-90	°C
Specific gravity	1.270 @ 25 °C	
Vapor density	5.17 (Air = 1)	
Vapour pressure	167 @ 25 °C	mm Hg

The exit gas from the reactor was passed through a coiled 1/4" copper thermophoresis tube, cooled by immersing the tube in an ice bath, to collect any product particles, then passing the exit gas into a NaOH scrubber to remove HCl and any unreacted MTS before releasing the stream into an extraction system.

A T-connection and valve assembly in the reactor outlet line enabled the selection between evacuation of the reactor tube or operation without vacuum whilst still providing a straight, unrestricted flow path form the reactor outlet to the phoresis tube for product collection.

Particle size distribution was determined through the use of a ZEN 3600 Malvern Zetasizer Nano System. Scanning electron microscopy (SEM) was performed on the particles using a high resolution (6 Å) JEOL 6000 system and transmission electron microscopy (TEM) was performed using the Phillips 301 instrument. Emission spectrographs were recorded with an Ocean Optics, HR 4000 High-Resolution Spectrometer. The optical input to the spectrometer for the emission lines was obtained by positioning the optical input cable onto the quartz tube.

Powder x-ray diffraction was conducted with a PANalytical X`pert Pro diffractometer using Co K_{α} radiation. The peak assignments were made using the databases supplied from the instrument manufacturer.

2.2 Experimental method

The argon plasma was initiated under vacuum ($2x10^{-3}$ mbar), using an Alcatel 2010I duel-stage rotary vane pump. The pressure was then gradually increased to atmospheric pressure where filamentation of the plasma structure occurred [29]. At this pressure the hydrogen and MTS were fed into the system. Depending on the hydrogen-to-MTS ratio, stable plasmas

could be maintained at applied powers between 200 and 1500 W. High hydrogen concentrations tended to starve and extinguish the plasma. High MTS content resulted in a "dusty" plasma [30]. Black powder deposited on the inner wall of the quartz tube and were removed after each experimental run using distilled water. The water was evaporated in a drying oven operating at 50 °C and the powders were collected.

The experimental parameters are shown in Table 2. All values were selected to cover a wide range of experimental parameters, within the capability of the system.

Table 2: Experimental parameters

Exp. number	Ar flow (sccm)	MTS flow (g/h)	H_2:MTS (mol:mol)	Power (W)
1	150	2.64	4.0	400
2	150	2.64	7.4	570
3	150	2.64	9.3	560
4	150	2.64	7.4	1300
5	150	2.64	4.0	1500
6	150	2.64	1.3	1300
7	150	2.64	0	870
8	150	2.64	1.3	570
9	150	2.64	4.0	950
10	150	2.64	4.0	950
11	150	2.64	4.0	950
12	150	2.64	4.0	1500

3. Results and discussion

The experimental results are shown in Table 3. Note that the enthalpy value given is the system enthalpy, which applies to all the components (argon, hydrogen and MTS) combined. The enthalpy values, H_{TOT} , were determined by Equation 2

$$H_{TOT} = \frac{P_f}{M_{TOT}} \quad (2)$$

where P_f is the forwarded power and M_{TOT} is the total mass flow rate. In general, particle agglomerates were obtained. The aggregate particle sizes (d_{50}) and the individual particle sizes obtained are both listed in Table 3. Experiment no. 3 yielded no results due to the continuous extinguishing of the plasma, the cause of which is expected to be the high H_2:MTS ratio of 9.3. As mentioned before, at these high levels the hydrogen tends to starve and extinguish the plasma. The running time is the total time measured from the point where MTS was introduced into the stable argon/hydrogen plasma (already operating at atmospheric pressure). The end of the time measurement was taken to be either after three minutes of stable operation or the longest time that a stable plasma could be maintained before extinguishing itself.

Based on the results, the best fitted-model included quadratic and 2-factor interaction terms. The analysis of variance (ANOVA) for the agglomerate sizes is presented in Table 4.

Table 3: Summary of experimental results.

Exp. number	Enthalpy (MJ/kg)	Average particle size of agglomerates, d_{50} (nm)	Average particle size of individual particles, d_{50} (nm)	Run Time (s)	SiC production rate (g/h)	SiC yield %
1	71.7	1296	89	18	1.40	14
2	101.6	1743	82	20	0.18	2
3	108.7	-	-	-	-	-
4	196.0	461	68	70	1.19	12
5	197.2	483	111	180	2.35	24
6	162.1	590	53	180	1.00	10
7	102.9	1233	132	180	0.56	6
8	102.7	800	132	180	2.25	23
9	152.4	744	110	223	0.74	9
10	152.4	634	131	148	0.87	9
11	152.4	675	91	180	1.20	12
12	215.1	475	121	180	0.74	7

Table 4: ANOVA for Response Surface quadratic model of Zetasizer results.

Source	Sum of Squares	Df	Mean Square	F Value	p-value Prob > F	
Model	1600171.00	5	320034.30	12.92	0.0070	Significant
A-Enthalpy	765238.10	1	765238.10	30.88	0.0026	
B-H_2:MTS	51635.30	1	51635.30	2.08	0.2085	
AB	177041.70	1	177041.70	7.14	0.0442	
A^2	42770.98	1	42770.98	1.73	0.2460	
B^2	194981.50	1	194981.50	7.87	0.0378	
Residual	123893.20	5	24778.65			
Lack of Fit	117712.60	3	39237.52	12.70	0.0739	Not significant
Pure Error	6180.67	2	3090.33			
Cor Total	1724065.00	10				

The ANOVA results indicate a model F-value of 12.92 and p-value < 0.05. Enthalpy has the greatest effect on the agglomerate sizes whereas H_2:MTS ratio was found to be least significant. In addition, the lack of fit of model was not significant. Model regression results are presented in Table 5.

Table 5: Model regression results for agglomerate sizes.

R-Squared	Adj R-Squared	Pred R-Squared	Adeq Precision
0.93	0.86	-0.05	11.07

The reasonable correlation coefficient (0.93) of the model indicates good agreement between the experimental and predicted data.

The analysis of variance (ANOVA) for the individual particle sizes is presented in Table 6.

Table 6: ANOVA for Response Surface quadratic model of SEM results.

Source	Sum of Squares	df	Mean Square	F Value	p-value Prob > F	
Model	2262.17	5	452.43	0.43	0.81	Not significant
A-Enthalpy	112.82	1	112.82	0.10	0.76	
B-H_2:MTS	585.03	1	585.03	0.56	0.49	
AB	661.22	1	661.22	0.63	0.46	
A^2	2.96	1	2.96	0.00	0.96	
B^2	762.94	1	762.94	0.73	0.43	
Residual	5211.65	5	1042.33			
Lack of Fit	4378.24	3	1459.41	3.50	0.23	Not significant
Pure Error	833.41	2	416.71			
Cor Total	7473.82	10				

The Model F-value of 0.43 implies the model is not significant relative to the noise. There is an 80.95 % chance that an F-value this large could occur due to noise. Values of "Prob > F" less than 0.0500 indicates the model terms are significant. In this case there are no significant model terms. Model regression results are presented in Table 7.

Table 7: Model regression results for individual particle sizes.

R-Squared	Adj R-Squared	Pred R-Squared	Adeq Precision
0.30	-0.39	-15.93	2.31

From these results it becomes clear that this model should not be used to navigate the design space, and caution is advised when doing so.

Application of response surface analysis (RSA) on the Zetasizer and SEM results yields the surface contour plots shown in Figure 4 and Figure 5 respectively. The individual particle size distribution indicates that the particle size decreases when the power and the H_2:MTS ratio increases. The agglomerate particle size distribution shows that, as expected, lower enthalpies produce larger agglomerates, but that the agglomeration process is much more sensitive to H_2:MTS ratios with higher ratios negatively influencing the agglomerate size.

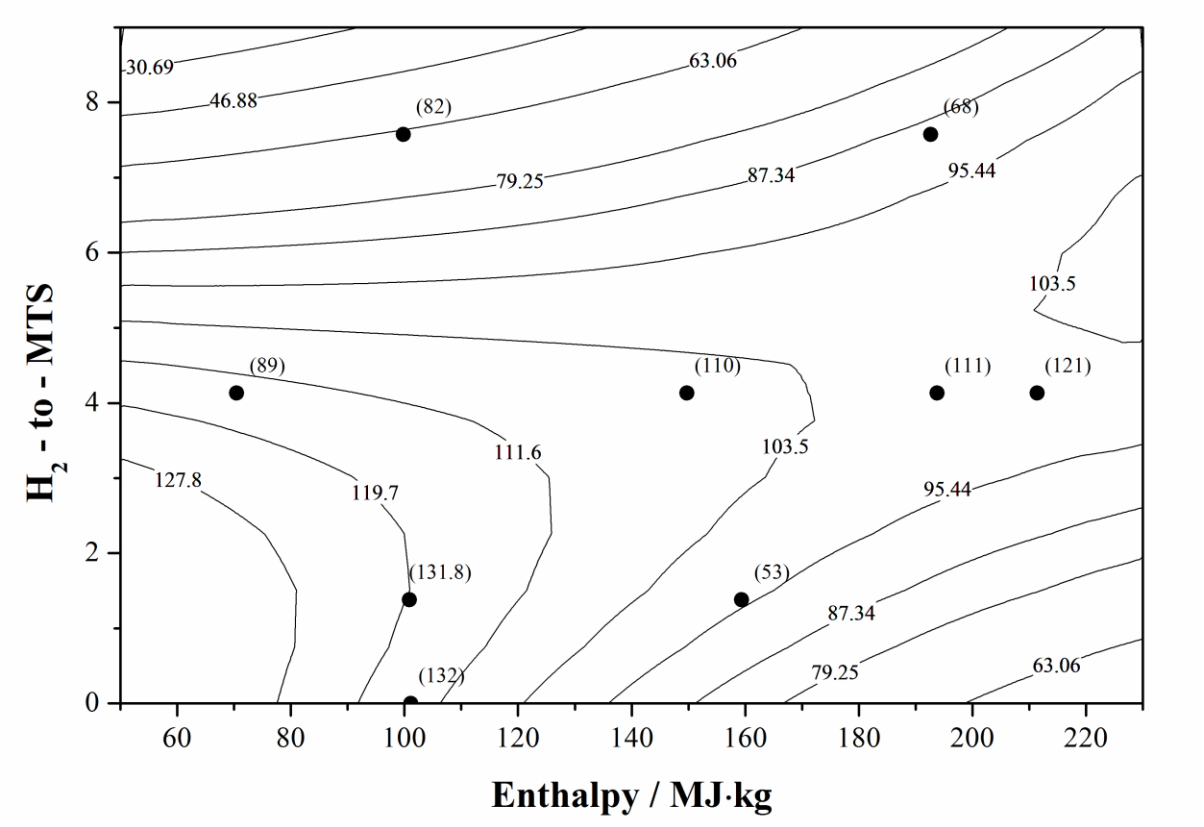

Figure 4: Effect of total enthalpy and H_2:MTS molar ratio on individual particle size.

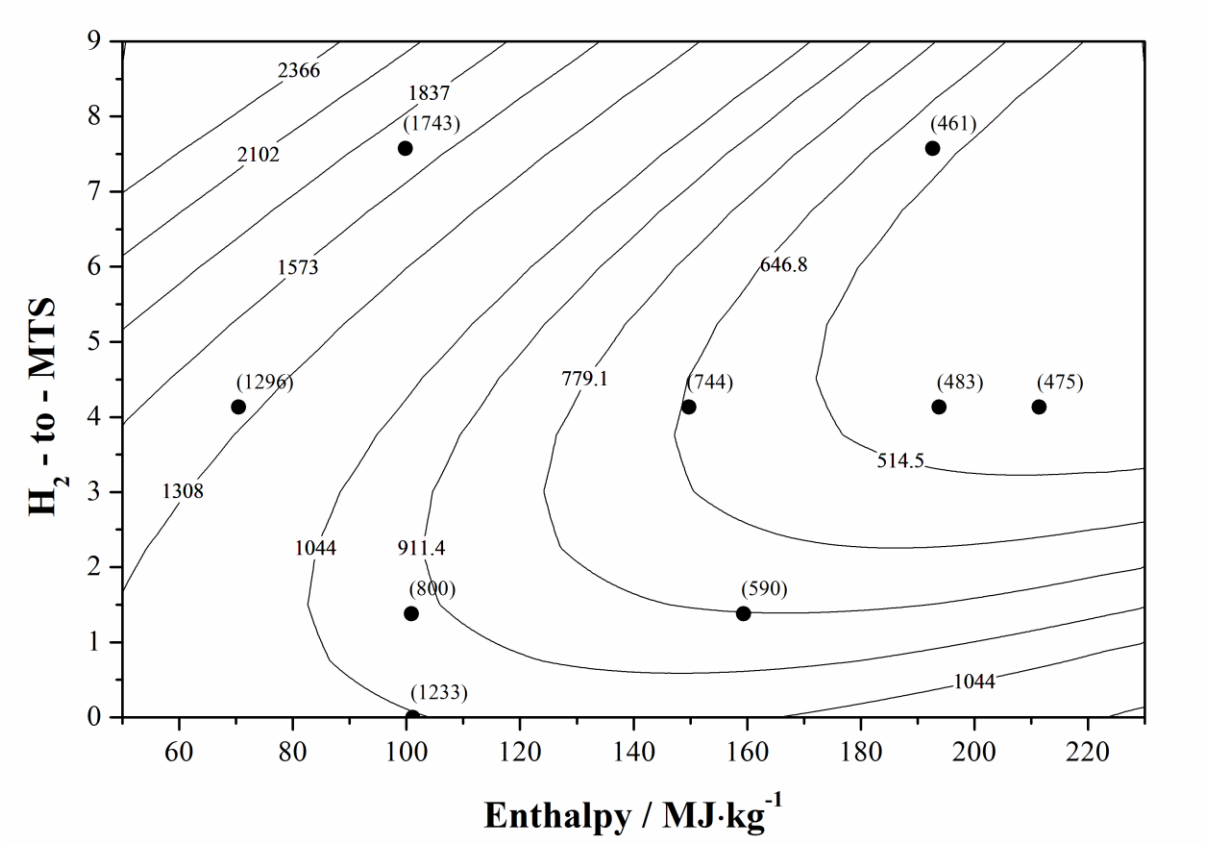

Figure 5: Effect of total enthalpy and H_2:MTS molar ratio on agglomerate size.

Figure 6 to Figure 9 present SEM and TEM micrographs, which show individual particle sizes of between 15 and 140 nm. These sizes are larger than those reported by Vennekamp *et al*. [16] who used tetramethylsilane (TMS) as precursor. Particles displayed a large degree of agglomeration, as is reflected in the large difference in SEM particle sizes when compared to the Zetasizer results.

Figure 6: SEM images of sample 11.

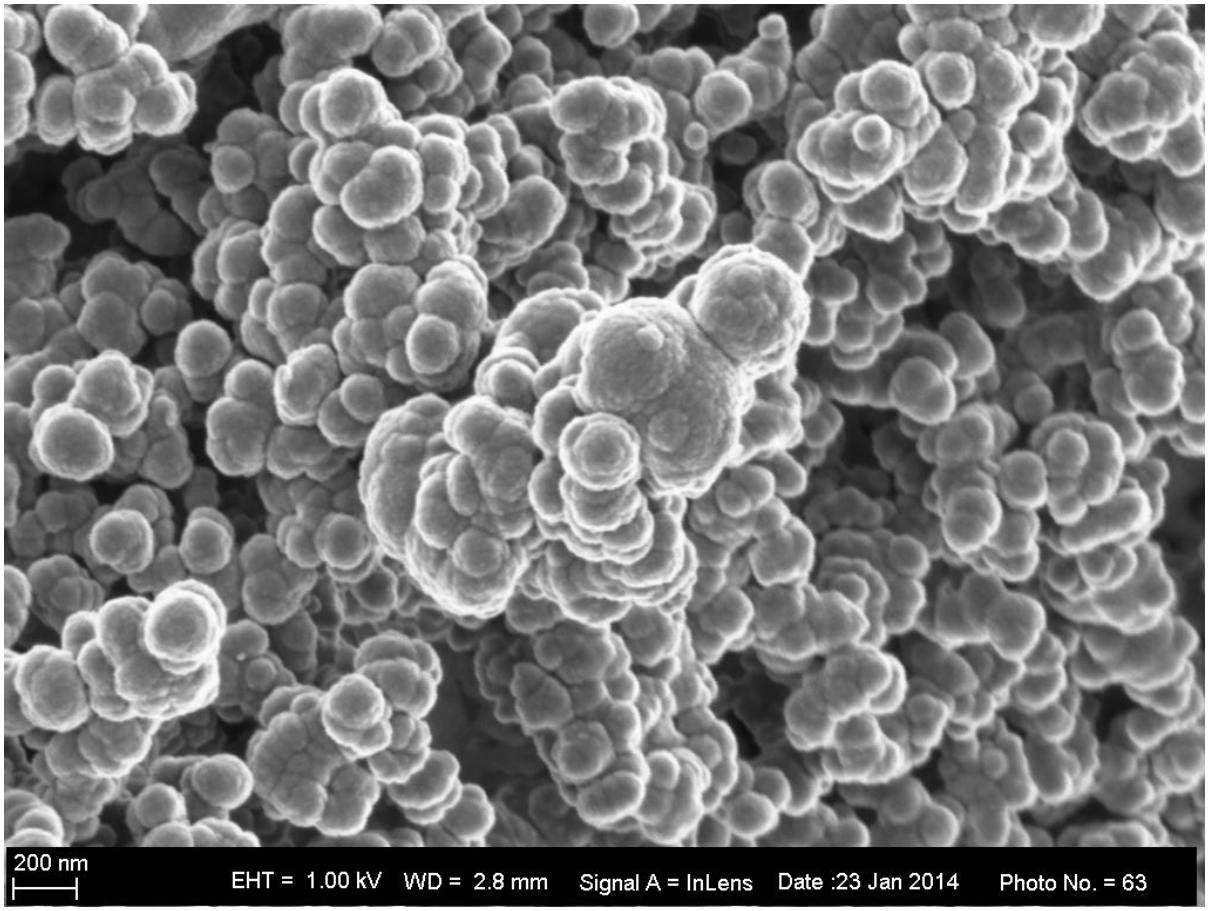

Figure 7: SEM image of sample 12.

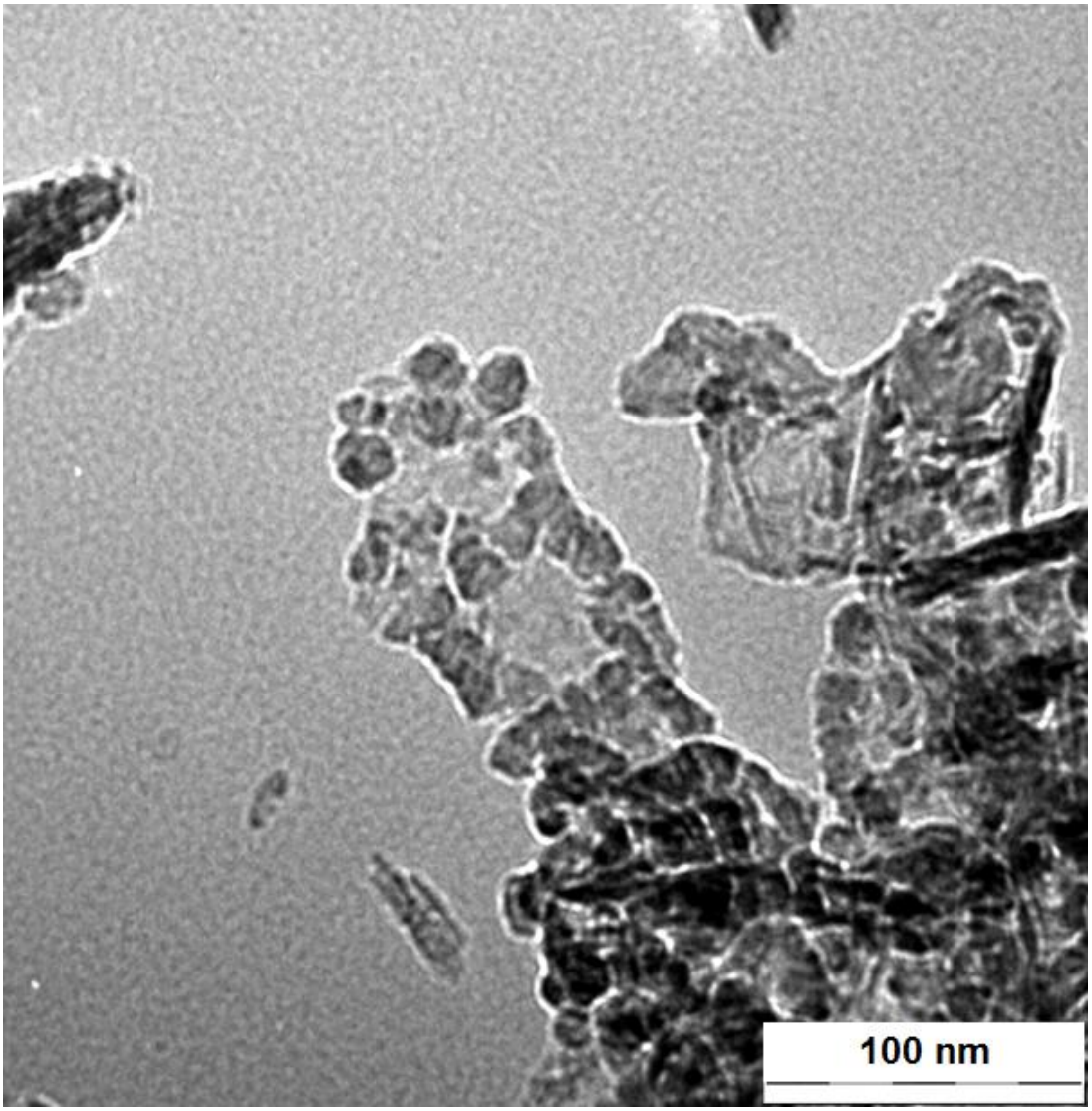

Figure 8: TEM image of sample 6.

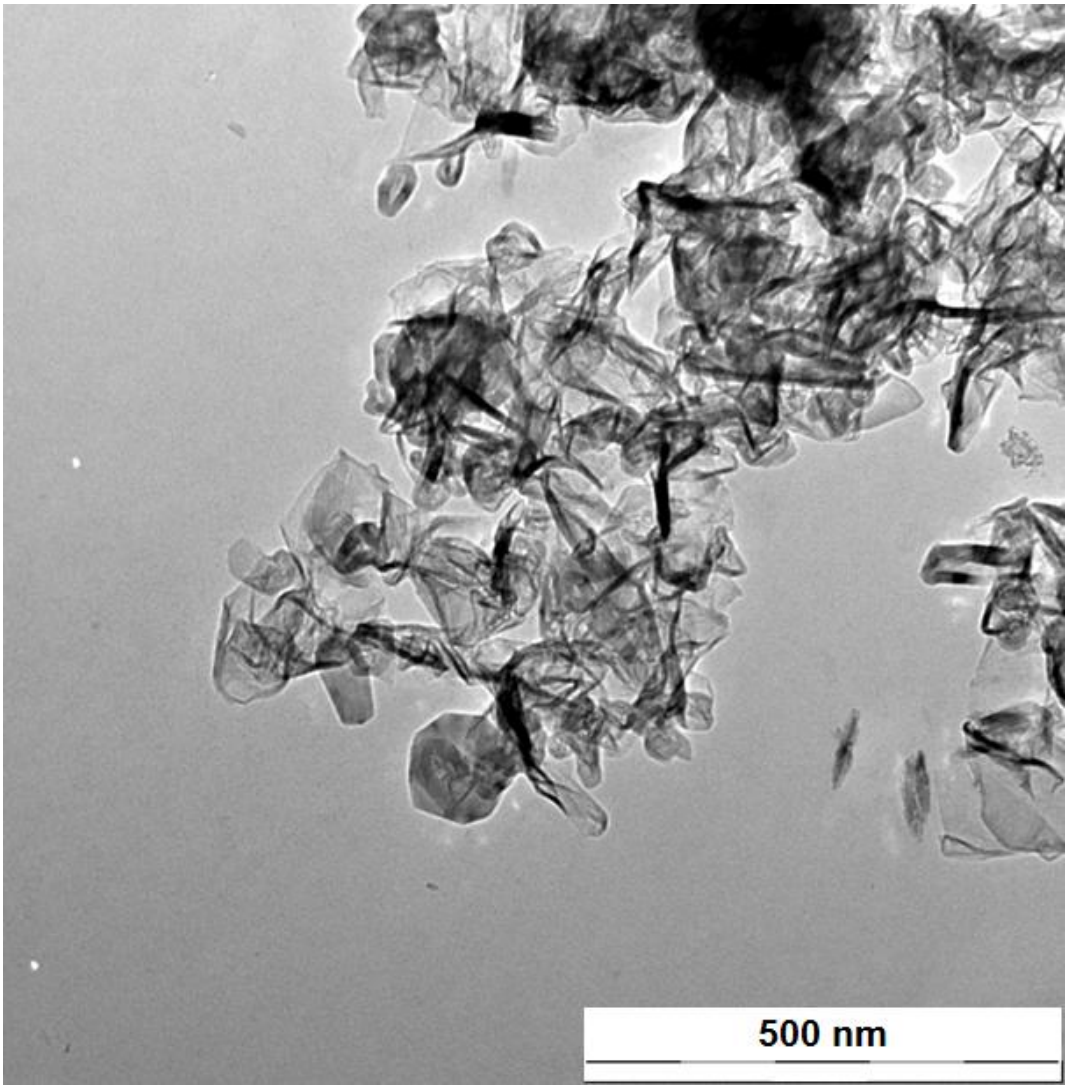

Figure 9: TEM image of sample 6.

Similar structures, with smaller particle sizes, were reported by Lin *et al*. [13] when operating at low pressures and using TMS. X-ray diffraction results show diffraction peaks at positions typical of β-SiC (cubic) as seen in Figure 10. Interestingly, the diffraction peaks for cubic silicon is also seen.

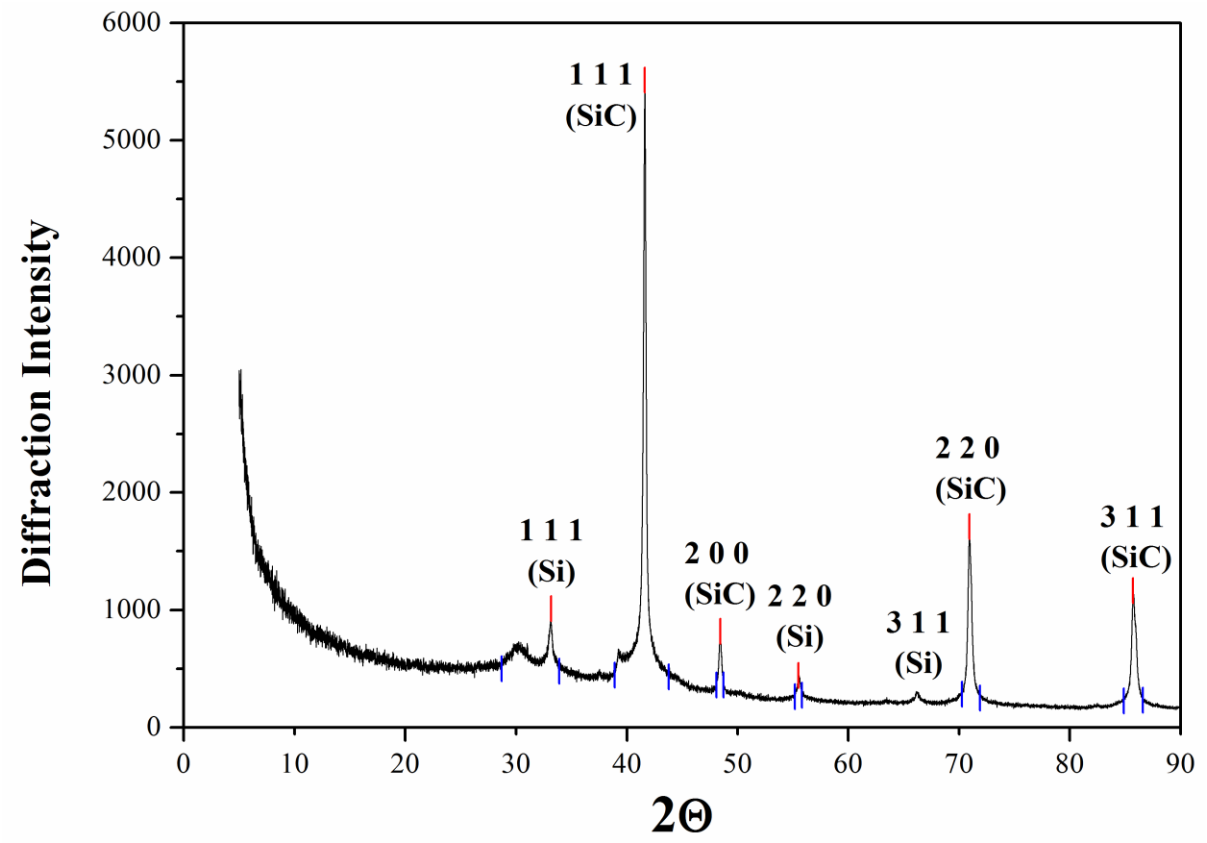

Figure 10: XRD spectrum of a product sample synthesised at an H_2:MTS ratio of 4. SiC refers to the β phase.

An optical emission spectrometer was used in order to determine the elements present in the plasma environment. This is a standard diagnostic tool often used to monitor discharge emissions [31]. An emission spectrum for wavelengths 200–1100 nm is shown in Figure 11. A few are obviously expected to be that of argon. The growth of nanoparticles in the plasma can drastically change the plasma properties. Layden *et al*. [32] performed optical emission spectroscopy on an RF sputtering discharge in argon during dust particle growth to analyse this change. They found that the intensities of all of the argon emission lines increase, indicating an increase in the number of high energy electrons as a result of particle growth. The majority of peaks in this case were in good agreement with experimental values of elementary silicon, carbon and argon [33]–[36], indicative of MTS decomposition in the plasma.

The presence of elementary silicon in the gas phase as well as silicon in the product material suggests that the addition of hydrogen to the plasma drives the conversion reactions too far into the reductive regime.

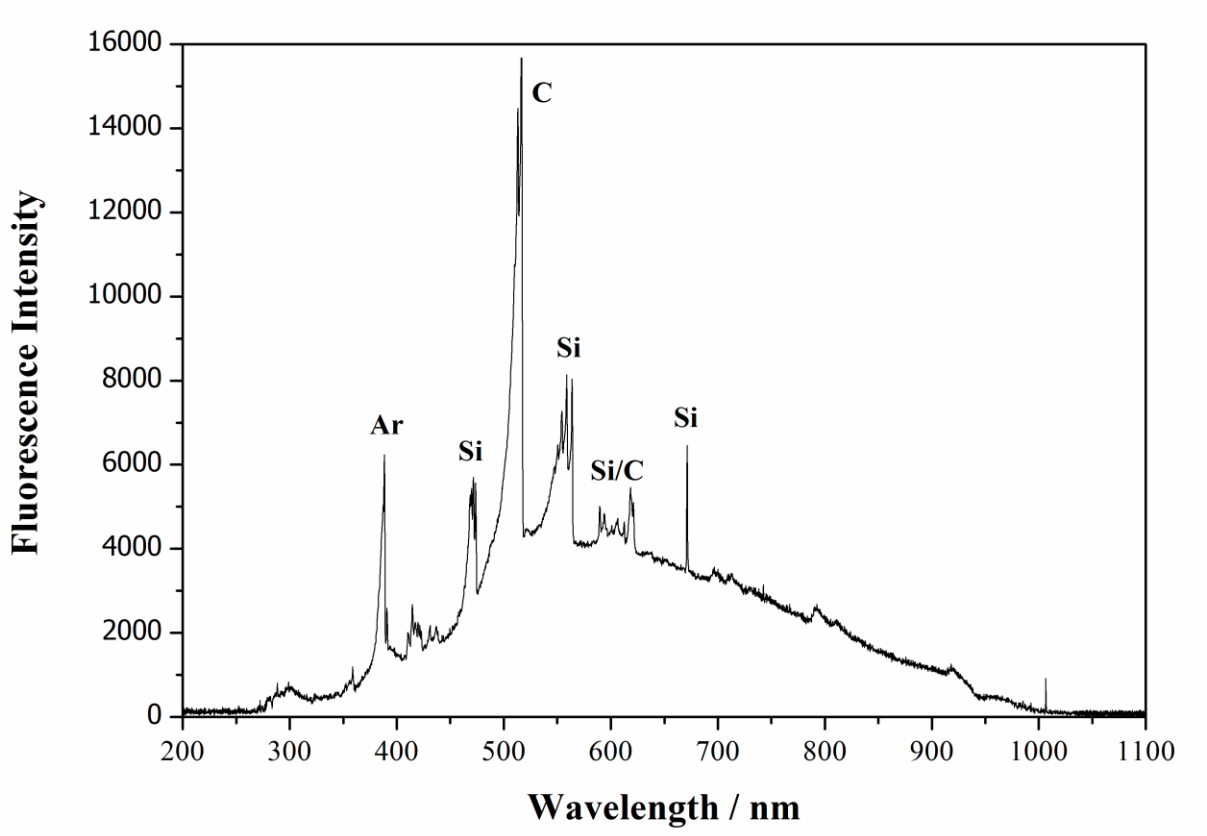

Figure 11: Emission spectrograph (Experiment 4).

The equilibrium thermodynamics and formation mechanisms of Equation 1 have been reported in the literature [37]. The optimum conditions for the formation of β-SiC are confirmed in Figure 12 using the thermodynamics software package TERRA [38]. At temperatures of around 1 400 K, optimum yield for β-SiC formation is obtained. Microwave plasmas can operate anywhere within the region of 1400–10 000 K [39]. This experiment operated between 1500 and 1900 K. Exact control of the gas temperature was not attempted or measured during this experiment due to the complicated nature of such an exercise. The enthalpy required to convert MTS into SiC is calculated using the assumption of thermodynamic equilibrium, shown in Figure 13. The experimental specific enthalpy values listed in Table 3 are significantly lower than the thermal values of Figure 13, suggesting that the non-equilibrium nature of the plasma plays a significant role in the MTS decomposition process.

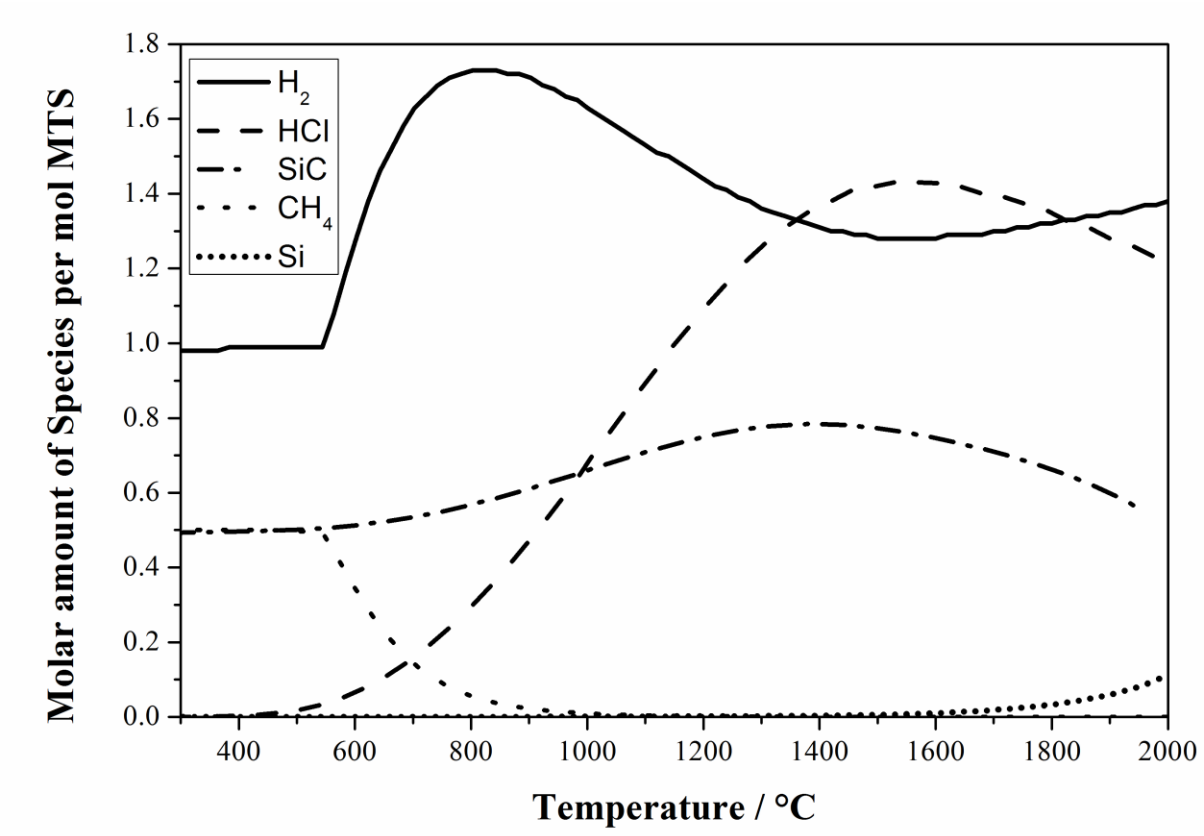

Figure 12: Equilibrium temperature dependent speciation curves.

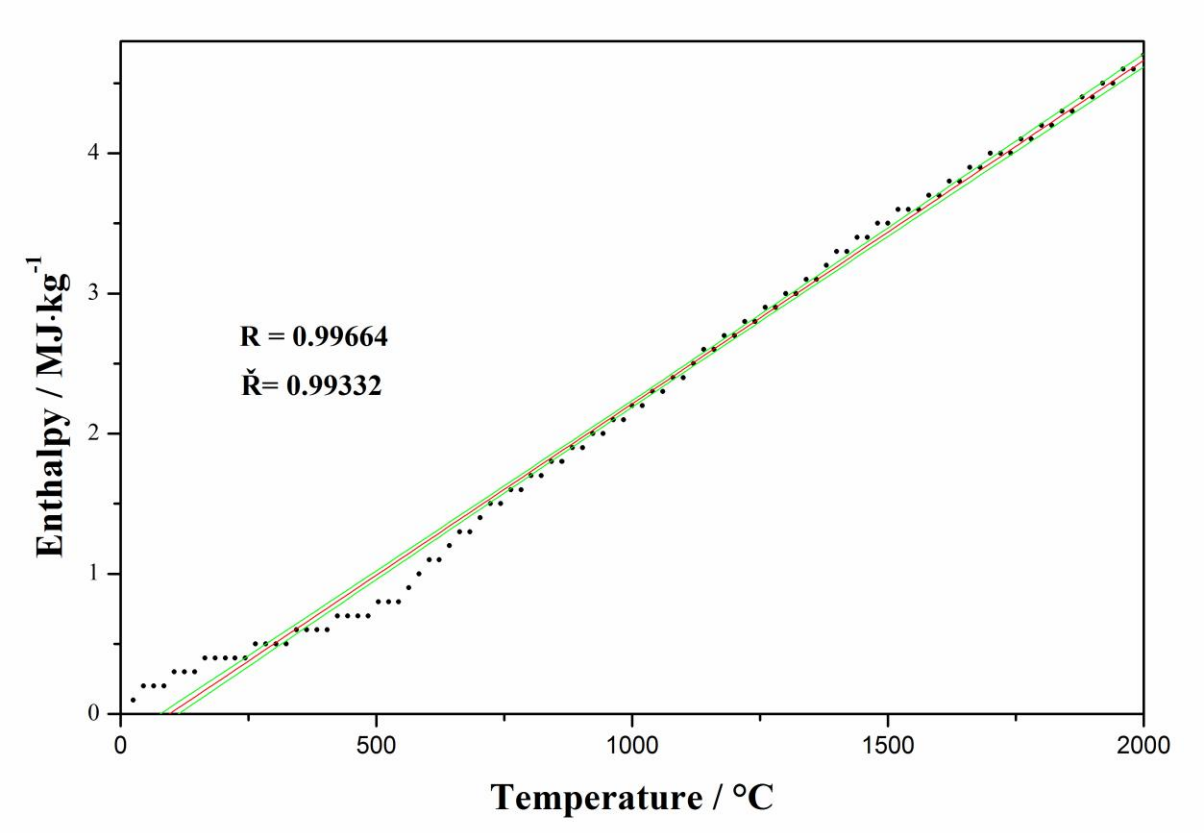

Figure 13: Specific enthalpy for MTS.

4. Conclusions

Methyltrichlosilane decomposes in a microwave plasma reactor to form SiC nanoparticles. Particle sizes range between 15 and 140 nm, confirmed by SEM and TEM characterization. These particles form agglomerates resulting in large particle sizes, as measured by Zetasizer. X-ray diffraction studies confirmed the presence of β-SiC and elemental Si in the product material. The process parameters studied were the H_2:MTS molar ratio and the total enthalpy. An inverse correlation was observed between enthalpy and the particle size. A similar correlation was observed for H_2:MTS ratio and particle size. The addition of hydrogen to the plasma complicates the production of pure SiC by the method reported here.

Acknowledgements: The authors acknowledge the South African National Research Foundation for financial support, and the South African Nuclear Energy Corporation for use of their equipment.

5. References

[1] G. L. Harris, *Properties of Silicon Carbide*. Washington DC, USA: INSPEC, 1995.

[2] S. Saddow and A. Agarwal, *Advances in silicon carbide processing and applications*. Norwood, USA: ARTECH HOUSE, INC, 2004.

[3] Y. Katoh, L. L. Snead, I. Szlufarska, and W. J. Weber, "Radiation effects in SiC for nuclear structural applications," *Curr. Opin. Solid State Mater. Sci.*, vol. 16, no. 3, pp. 143–152, 2012.

[4] S. Dhage, H.-C. Lee, M. S. Hassan, M. S. Akhtar, C.-Y. Kim, J. M. Sohn, K.-J. Kim, H.-S. Shin, and O.-B. Yang, "Formation of SiC nanowhiskers by carbothermic reduction of silica with activated carbon," *Mater. Lett.*, vol. 63, no. 2, pp. 174–176, Jan. 2009.

[5] D. B. Chrisey and G. K. Hubler, *Pulsed Laser Deposition of Thin Films*. New York: Wiley & Sons, 1994.

[6] J. Li, J. Tian, and L. Dong, "Synthesis of SiC precursors by a two-step sol-gel process and their conversion to SiC powders," *J. Eur. Cermaic Soc.*, vol. 77, pp. 1853–1857, 2000.

[7] L. N. Satapathy, P. D. Ramesh, D. Agrawal, and R. Roy, "Microwave synthesis of phase-pure , fine silicon carbide powder," *Mater. Res. Bull.*, vol. 40, no. 2005, pp. 1871–1882, 2005.

[8] B. M. Moshtaghioun, R. Poyato, F. L. Cumbrera, S. de Bernardi-Martin, A. Monshi, M. H. Abbasi, F. Karimzadeh, and A. Dominguez-Rodriguez, "Rapid carbothermic synthesis of silicon carbide nano powders by using microwave heating," *J. Eur. Ceram. Soc.*, vol. 32, no. 8, pp. 1787–1794, Jul. 2012.

[9] Z. Károly, I. Mohai, S. Klébert, a. Keszler, I. E. Sajó, and J. Szépvölgyi, "Synthesis of SiC powder by RF plasma technique," *Powder Technol.*, vol. 214, no. 3, pp. 300–305, Dec. 2011.

[10] H. Sachdev and P. Scheid, "Formation of silicon carbide and silicon carbonitride by RF-plasma CVD," *Diam. Relat. Mater.*, vol. 10, no. 3–7, pp. 1160–1164, Mar. 2001.

[11] S.-M. Ko, S.-M. Koo, W.-S. Cho, K.-T. Hwnag, and J.-H. Kim, "Synthesis of SiC nano-powder from organic precursors using RF inductively coupled thermal plasma," *Ceram. Int.*, vol. 38, no. 3, pp. 1959–1963, Apr. 2012.

[12] B. Kim and B. Lee, "Effect of Plasma and Control Parameters on SiC Etching in a C 2 F 6 Plasma," *Plasma Chem. Plasma Process.*, vol. 23, no. 3, pp. 489–499, 2003.

[13] H. Lin, J. A. Gerbec, M. Sushchikh, and E. W. Mcfarland, "Synthesis of amorphous silicon carbide nanoparticles in a low temperature, low pressure plasma reactor," *Nanotechnology*, vol. 19, no. 325601, pp. 1–8, 2008.

[14] C. Tang, L. Fu, a. J. S. Fernandes, M. J. Soares, G. Cabral, a. J. Neves, and J. Grácio, "Simultaneous formation of silicon carbide and diamond on Si substrates by microwave plasma assisted chemical vapor deposition," *New Carbon Mater.*, vol. 23, no. 3, pp. 250–258, Mar. 2008.

[15] S. Honda, Y.-G. Baek, T. Ikuno, H. Kohara, M. Katayama, K. Oura, and T. Hirao, "SiC nanofibers grown by high power microwave plasma chemical vapor deposition," *Appl. Surf. Sci.*, vol. 212–213, pp. 378–382, May 2003.

[16] M. Vennekamp, I. Bauer, M. Groh, E. Sperling, S. Ueberlein, M. Myndyk, G. Mäder, and S. Kaskel, "Formation of SiC nanoparticles in an atmospheric microwave plasma," *Beilstein J. Nanotechnol.*, vol. 2, pp. 665–673, 2011.

[17] J. Knipping, H. Wiggers, B. Rellinghaus, P. Roth, D. Konjhodzic, and C. Meier, "Synthesis of High Purity Silicon Nanoparticles in a Low Pressure Microwave Reactor," *J. Nanosci. Nanotechnol.*, vol. 4, no. 8, pp. 1039–1044, 2004.

[18] D. Vollath and D. V Szabo, "Synthesis of nanocrystalline MoS2 and WS2 in a microwave plasma," *Mater. Lett.*, vol. 35, pp. 236–244, 1998.

[19] Y. Hattori, S. Nomura, S. Mukasa, H. Toyota, T. Inoue, and T. Kasahara, "Synthesis of tungsten trioxide nanoparticles by microwave plasma in liquid and analysis of physical properties," *J. Alloys Compd.*, vol. 560, pp. 105–110, May 2013.

[20] A. Irzh, I. Genish, L. Klein, L. a Solovyov, and A. Gedanken, "Synthesis of ZnO and Zn nanoparticles in microwave plasma and their deposition on glass slides.," *Langmuir*, vol. 26, no. 8, pp. 5976–84, Apr. 2010.

[21] H. Sone, T. Kaneko, and N. Miyakawa, "In situ measurements and growth kinetics of silicon carbide chemical vapor deposition from methyltrichlorosilane," *J. Cryst. Growth*, vol. 219, no. 3, pp. 245–252, Oct. 2000.

[22] G. D. Papasouliotis and S. V. Sotirchos, "Experimental study of atmospheric pressure chemical vapor deposition of silicon carbide from methyltrichlorosilane," *J. Mater. Res.*, vol. 14, no. 08, pp. 3397–3409, Jan. 2011.

[23] T. Kaneko, N. Miyakawa, H. Sone, and H. Yamazaki, "Growth kinetics of hydrogenated amorphous silicon carbide films by RF plasma-enhanced CVD using two kinds of source materials," *Thin Solid Films*, vol. 409, no. 1, pp. 74–77, Apr. 2002.

[24] X. Wang, K. Su, J. Deng, Y. Liu, Y. Wang, Q. Zeng, L. Cheng, and L. Zhang, "Initial decomposition of methyltrichlorosilane in the chemical vapor deposition of silicon-carbide," *Comput. Theor. Chem.*, vol. 967, no. 2–3, pp. 265–272, Aug. 2011.

[25] D. Jaglin, J. Binner, B. Vaidhyanathan, C. Prentice, B. Shatwell, and D. Grant, "Microwave Heated Chemical Vapor Infiltration: Densification Mechanism of SiCf/SiC Composites," *J. Am. Ceram. Soc.*, vol. 2717, p. 060613004617005–???, Jun. 2006.

[26] L. Zhong and L. Hou, “Nano-Structured Si-C-N Composite Powder Produced by Radio Frequency Induction Plasma and its Microwave Absorbing Properties,” *J. Eng. Sci. Technol. Rev.*, vol. 6, no. 12, pp. 160–163, 2013.

[27] S. H. Mousavipour, V. Saheb, and S. Ramezani, “Kinetics and Mechanism of Pyrolysis of Methyltrichlorosilane †,” *J. Phys. Chem. A*, vol. 108, no. 11, pp. 1946–1952, Mar. 2004.

[28] C. L. Yaws, *Yaws’ Critical Property Data for Chemical Engineers and Chemists*. New York: Knovel, 2014.

[29] R. P. Cardoso, T. Belmonte, C. Noël, F. Kosior, and G. Henrion, “Filamentation in argon microwave plasma at atmospheric pressure,” *J. Appl. Phys.*, vol. 105, no. 9, 2009.

[30] P. Shukla and A. Mamun, *Introduction to Dusty Plasma Physics*. Cornwall: Institute of Physics Publishing, 2002.

[31] J. Cooper, “Plasma spectroscopy,” *Reports Prog. Phys.*, vol. 29, no. 1, p. 35, 1966.

[32] B. Layden, V. Cheung, and A. A. Samarian, “Effect of Dust Particle Growth on the Emission Spectrum of a Complex Plasma,” *IEEE Trans. Plasma Sci.*, vol. X, no. X, pp. 6–7, 2011.

[33] A. Kramida, Y. Ralchenko, J. Reader, and NIST ASD Team, “NIST Atomic Spectra Database (ver. 5.2),” 2014. [Online]. Available: http://physics.nist.gov/asd. [Accessed: 23-Oct-2014].

[34] K. Wagatsuma and K. Hirokawa, “Characterization of Atomic Emission Lines from Argon , Neon , and Nitrogen Glow Discharge Plasmas,” *Anal. Chem.*, vol. 57, pp. 2901–2907, 1985.

[35] M. Milan and J. J. U. Laserna, “Diagnostics of silicon plasmas produced by visible nanosecond laser ablation,” *Spectrochim. Acta Part B At. Spectrosc.*, vol. 56, pp. 275–288, 2001.

[36] L. Di, J.-R. Shi, S.-J. Wang, Q.-L. Dong, J. Zhao, Y.-T. Li, J. Fu, F.-D. Wang, Y.-J. Shi, B.-N. Wan, G. Zhao, and J. Zhang, “Emission Lines of Boron, Carbon, Oxygen and Iron in Tokamak Plasma,” *Chinese Phys. Lett.*, vol. 28, no. 7, p. 075201, Jul. 2011.

[37] J. Deng, K. Su, X. Wang, Q. Zeng, L. Cheng, Y. Xu, and L. Zhang, “Thermodynamics of the gas-phase reactions in chemical vapor deposition of silicon carbide with methyltrichlorosilane precursor,” *Theor Chem Acc.*, vol. 122, pp. 1–22, 2009.

[38] B. Trusov, “Terra - Phase and Chemical Equilibrium of Multicomponent Systems.” Bauman Moscow State Technical University, Moscow, 2006.

[39] C. Tendero, C. Tixier, P. Tristant, J. Desmaison, and P. Leprince, “Atmospheric pressure plasmas: A review,” *Spectrochim. Acta Part B At. Spectrosc.*, vol. 61, no. 1, pp. 2–30, Jan. 2006.